

MPC Based Linear Equivalence with Control Barrier Functions for VTOL-UAVs

Ali Mohamed Ali, Hashim A. Hashim, and Chao Shen

Abstract—In this work, we propose a cascaded scheme of linear Model prediction Control (MPC) based on Control Barrier Functions (CBF) with Dynamic Feedback Linearization (DFL) for Vertical Take-off and Landing (VTOL) Unmanned Aerial Vehicles (UAVs). CBF is a tool that allows enforcement of forward invariance of a set using Lyapunov-like functions to ensure safety. The First control synthesis that employed CBF was based on Quadratic Program (QP) that modifies the existing controller to satisfy the safety requirements. However, the CBF-QP-based controllers leading to longer detours and undesirable transient performance. Recent contributions utilize the framework of MPC benefiting from the prediction capabilities and constraints imposed on the state and control inputs. Due to the intrinsic nonlinearities of the dynamics of robotics systems, all the existing MPC-CBF solutions rely on nonlinear MPC formulations or operate on less accurate linear models. In contrast, our novel solution unlocks the benefits of linear MPC-CBF while considering the full underactuated dynamics without any linear approximations. The cascaded scheme converts the problem of safe VTOL-UAV navigation to a Quadratic Constraint Quadratic Programming (QCQP) problem solved efficiently by off-the-shelf solvers. The closed-loop stability and recursive feasibility is proved along with numerical simulations showing the effective and robust solutions.

Index Terms—Unmanned Aerial Vehicles, Vertical Take-off and Landing, Model Predictive Control, MPC, Nonlinearity, Dynamic Feedback Linearization, Optimal Control.

I. INTRODUCTION

The urban applications of Vertical Take-off and Landing (VTOL) Unmanned Aerial Vehicles (UAVs) highlight the significance of obstacle avoidance and hence classify VTOL-UAV navigation as a safety-critical system (visit Fig.1) [1], [2]. The term safety-critical is used by researchers to distinguish systems for which safety is a major design consideration [3]. The study of safety in dynamical systems started in [4], where the necessary and sufficient conditions of the invariant set were studied [5]. Recently, the Control Barrier Function (CBF) was introduced as a Lyapunov-like function that represents a safety measure of the system [3], [6]. CBF-based safety constraints were then utilized to construct a Quadratic Program (QP) minimizing the difference between the feedback controller and the applied controller under the CBF inequality constraint. The CBF-QP approach has been adopted to solve many control problems such as lane keeping [3], safe navigation of a quadcopter [7], haptic teleoperation [8], and others.

This work was supported in part by the National Sciences and Engineering Research Council of Canada (NSERC), under the grants RGPIN-2022-04937, RGPIN-2022-04940, DGEGR-2022-00103 and DGEGR-2022-00106.

A. M. Ali and H. A. Hashim are with the Department of Mechanical and Aerospace Engineering, Carleton University, Ottawa, ON, K1S-5B6, Canada (e-mail: AliMohamedAli@email.carleton.ca and hhashim@carleton.ca). C. Shen is with the Department of Systems and Computer Engineering, Carleton University, Ottawa, ON, K1S-5B6, Canada (shenchao@sce.carleton.ca).

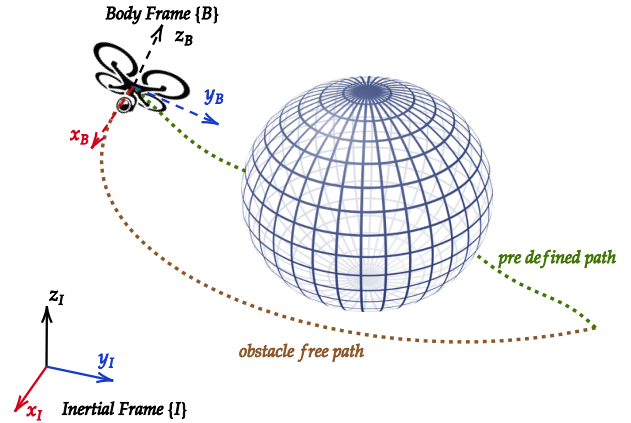


Fig. 1: VTOL-UAV safe navigation task where $\{I\}$ is the body fixed frame and $\{B\}$ is the Global frame

The advantage of MPC, also known as receding horizon control, consists in the strong ability to handle input and states constraints. Thus, it is widely used for many robotic systems. In [9], [10] safety was considered in the MPC framework as an extra distance constraint with various Euclidean norms in the optimization problem. However, the obstacle avoidance constrains used by these approaches get activated and change the robot's trajectory only if the robot is in close proximity to an obstacle. As such, avoiding obstacles located further away requires larger prediction horizon leading to higher computational time [11]. Nonetheless, the majority of existing literature uses a simplified model of the dynamics, for instance [12] solves the lane keep problem using a linear passenger car model to formulate the MPC optimization. Recently promising efforts have been made to combine MPC and CBFs. In [13], the authors proposed achieving vehicle safety by incorporating continuous-time CBFs into discrete-time MPC. In [14], the authors proposed a control design that leverages CBFs for low-level control and nonlinear MPC policies for high-level planning. This method treats MPC and CBF separately utilizing them at different levels of the solution to control the nonlinear model of Segway and for legged robots in [15]. In [11], a discrete formulation of the CBF was unified with nonlinear MPC and applied to the car racing problem. In [16], the MPC based CBF was converted to an iterative convex optimization by linearizing the nonlinear dynamics as well as the CBF. Collision avoidance for VTOL-UAVs has been investigated in [17] where a combination of geometrical constraints and kinematics was used. In [18] the authors proposed a similar framework of the artificial potential fields, where Tangent Vec-

tor Field Guidance (TVFG) algorithms employed to generate obstacle-free path for VTOL-UAVs. Vision-based detection and collision avoidance have been widely studied [19]. The work in [19] proposed an MPC-based control with vision-based detection of obstacles. However, the shortcoming of vision-based MPC approaches for collision avoidance consists in VTOL-UAV starting to deviate from an obstacle only when it is in its close proximity requiring larger prediction horizon.

Contributions: The proposed solution bridges the above-identified literature gaps by formulating MPC using CBF to control the VTOL-UAV such that the safety constraint gets activated everywhere providing smooth trajectory with the constraints are likely to be satisfied compared to usage of Euclidean norms as a constraint. The CBF provides the notion of the global forward invariance of the safe set. The VTOL-UAV avoids the obstacle even if it is far from it leading to a shorter prediction horizon, unlike the Euclidean distance case where the constraint is activated once it near the obstacle. Our proposed MPC-CBF with DFL considers the full nonlinear underactuated UAV model. To address the system nonlinearities and the computational complexity arising from the nonlinear MPC, we introduce a solution that integrates a cascaded scheme of Dynamic Feedback Linearization (DFL) with MPC unlocking the benefits of linear MPC as opposed to nonlinear MPC in terms of computational burden and stability guarantees. The contribution of this work can be summarized as follows:

- 1) A cascaded scheme of DFL and MPC is proposed to unlock the benefits associated with Linear MPC.
- 2) The mapping between the original nonlinear underactuated model and the linear equivalent model (MPC-CBF formulation designed on linear equivalent model by DFL) is presented. Combining MPC-CBF and DFL into a single scheme allows us to convert the safe navigation of the VTOL-UAV full model into a Quadratic Constraint Quadratic Programming (QCQP) Problem.
- 3) Closed Loop stability and recursive feasibility of the proposed scheme is proved and numerical simulations for a standard safe navigation task of a VTOL-UAV are carried out demonstrating the effectiveness and robustness of the proposed scheme.

The remainder of the paper is organized as follows: Section II presents preliminaries and mathematical notation. Section III introduces the VTOL-UAV dynamic model. The linear equivalence model is discussed in Section IV. Section V presents the proposed control scheme. Section VI illustrates the effectiveness of the proposed scheme through numerical simulations. Finally, Section VII concludes the work.

II. PRELIMINARIES

In this paper, \mathbb{R} denotes the set of real numbers and \mathcal{L} defines the Lie derivative operator. For a given vector field $f(x)$ such that $f : \mathbb{R}^n \rightarrow \mathbb{R}^n$ and a scalar function $\lambda : \mathbb{R}^n \rightarrow \mathbb{R}$, the Lie derivative of λ with respect to f can be written as

$\mathcal{L}_f \lambda = \frac{\partial \lambda}{\partial x} \cdot f(x)$. Consider the following single input single output nonlinear affine in control system:

$$\begin{cases} \dot{x} &= f(x) + g(x)u \\ y &= h(x) \end{cases} \quad (1)$$

where $x \in \mathbb{R}^n$ describes the system states, $u \in \mathbb{R}$ defines the system control input, $y \in \mathbb{R}$ denotes the system output, $f : \mathbb{R}^n \rightarrow \mathbb{R}^n$, $g : \mathbb{R}^n \rightarrow \mathbb{R}^n$, and $h : \mathbb{R}^n \rightarrow \mathbb{R}$. The relative degree r of such system can be defined at point x_0 if $\mathcal{L}_g \mathcal{L}_f^\rho h(x) = 0$ for all x in the neighborhood of x_0 , $\rho < r - 1$, and $\mathcal{L}_g \mathcal{L}_f^{r-1} h(x_0) \neq 0$. The multi-input multi-output (MIMO) square affine in control system is expressed as follows:

$$\begin{cases} \dot{x} &= f(x) + g_1(x)u_1 + \dots + g_m(x)u_m \\ y_1 &= h_1(x) \\ \vdots &= \vdots \\ y_m &= h_m(x) \end{cases} \quad (2)$$

where $x \in \mathbb{R}^n$ describes the system states, $u \in \mathbb{R}^m$ defines the system control input, $y \in \mathbb{R}^m$ denotes the system output, $f : \mathbb{R}^n \rightarrow \mathbb{R}^n$, $g : \mathbb{R}^n \rightarrow \mathbb{R}^m$, and $h : \mathbb{R}^n \rightarrow \mathbb{R}^m$.

Lemma 1. [20] *The relative degree of (2) at x_0 is described as $r = [r_1, \dots, r_m]^T \in \mathbb{R}^m$ exists if:*

- $\mathcal{L}_{g_j} \mathcal{L}_f^\rho h_i(x) = 0$ at the neighborhood of x_0 for all $1 \leq j \leq m$, $\rho < r_i - 1$, and $1 \leq i \leq m$.
- The decoupling matrix $A(x) \in \mathbb{R}^{m \times m}$ defined as

$$A(x) = \begin{pmatrix} \mathcal{L}_{g_1} \mathcal{L}_f^{r_1-1} h_1(x) & \dots & \mathcal{L}_{g_m} \mathcal{L}_f^{r_1-1} h_1(x) \\ \mathcal{L}_{g_1} \mathcal{L}_f^{r_2-1} h_2(x) & \dots & \mathcal{L}_{g_m} \mathcal{L}_f^{r_2-1} h_2(x) \\ \dots & \dots & \dots \\ \mathcal{L}_{g_1} \mathcal{L}_f^{r_m-1} h_m(x) & \dots & \mathcal{L}_{g_m} \mathcal{L}_f^{r_m-1} h_m(x) \end{pmatrix} \quad (3)$$

is nonsingular at $x = x_0$.

Lemma 2. [20] *The input-to-state feedback linearization of the system dynamics in (2) is solvable at x_0 using the control*

$$\text{input } u = A^{-1}(x) \left(\begin{bmatrix} -\mathcal{L}_f^{r_1} h_1(x) \\ \vdots \\ -\mathcal{L}_f^{r_m} h_m(x) \end{bmatrix} + \begin{bmatrix} v_1 \\ \vdots \\ v_m \end{bmatrix} \right), \text{ if } \sum_{r=1}^m r = n$$

and the decoupling input matrix $A(x)$ in (3) is of full rank. v is an external reference input to be defined.

Throughout this paper $\mathcal{H}(x)$ represents a control barrier function with $\mathcal{H}(x) : D \subset \mathbb{R}^n \rightarrow \mathbb{R}_{\geq 0}$ describing a safety metric. The class of \mathcal{K}_∞ extended function is denoted by κ such that it is a strictly increasing function with the mapping $[0, \infty) \rightarrow [0, \infty)$ and $\lim_{r \rightarrow \infty} \kappa(r) = \infty$. Define $C = \{x \in D \subset \mathbb{R}^n : \mathcal{H}(x) \geq 0\}$ to be the safe set.

III. VTOL-UAV DYNAMIC MODEL

The Euler angles $\zeta = [\phi, \theta, \psi]^T \in \mathbb{R}^3$ mapping to rotational matrix $R \in SO(3)$ follows $R_\zeta : \mathbb{R}^3 \rightarrow SO(3)$ [21]:

$$R_\zeta = \begin{bmatrix} c_\psi c_\theta & c_\psi s_\theta s_\phi - c_\phi s_\psi & s_\phi s_\psi + c_\phi c_\psi s_\theta \\ c_\theta s_\psi & c_\phi c_\psi + s_\phi s_\psi s_\theta & c_\phi s_\psi s_\theta - c_\psi s_\phi \\ -s_\theta & c_\theta s_\phi & c_\phi c_\theta \end{bmatrix} \quad (4)$$

with $c = \cos$, $s = \sin$, and $t = \tan$. The dynamics of a rigid-body under external forces applied to the center of mass and expressed in Newton-Euler formalism are defined as follows:

$$\sum F = m\dot{V} \quad F, V \in \{\mathcal{I}\} \quad (5)$$

$$\sum M = J\dot{\Omega} + \Omega \times J\Omega \quad M, \Omega \in \{\mathcal{B}\} \quad (6)$$

where $V = [v_x, v_y, v_z]^\top$ is the linear velocity vector, $\Omega = [\Omega_x, \Omega_y, \Omega_z]^\top$ is rotational velocity, m is the total mass of the UAV, J is the UAV inertia matrix, $\{\mathcal{I}\}$ denotes inertial-frame, and $\{\mathcal{B}\}$ refers to body-frame. $\sum F$ and $\sum M$ are the sum of external forces and moments acting on the UAV. The full nonlinear underactuated model (neglecting the aerodynamic forces) can be written in the form of MIMO affine in control system as in (2) with $x = [p_x, p_y, p_z, \phi, \theta, \psi, v_x, v_y, v_z, \dot{\phi}, \dot{\theta}, \dot{\psi}]^\top \in \mathbb{R}^{12}$ being a state vector and the functions $f(x)$, $g_1(x)$, $g_2(x)$, $g_3(x)$, and $g_4(x)$ being expressed as follows [22]:

$$f(x) = \begin{bmatrix} V \\ \dot{\theta} s_\phi \sec \theta + \dot{\psi} c_\phi \sec \theta \\ \dot{\theta} c_\phi - \dot{\psi} s_\phi \\ \dot{\phi} + \dot{\theta} s_\phi t_\theta + \dot{\psi} c_\phi t_\theta \\ 0 \\ 0 \\ -g \\ \frac{I_y - I_z}{I_x} \dot{\theta} \dot{\psi} \\ \frac{I_z - I_x}{I_y} \dot{\phi} \dot{\psi} \\ \frac{I_x - I_y}{I_z} \dot{\phi} \dot{\theta} \end{bmatrix}, g_1(x) = \begin{bmatrix} 0_{1 \times 6} \\ \frac{-(c_\phi c_\theta s_\psi + s_\phi s_\psi)}{m} \\ \frac{-(c_\phi c_\theta s_\psi + s_\phi s_\psi)}{m} \\ \frac{c_\theta c_\phi}{m} \\ 0_{1 \times 3} \end{bmatrix}$$

$$g_2(x) = \begin{bmatrix} 0_{1 \times 9} \\ \frac{d}{I_x} \\ 0_{1 \times 2} \end{bmatrix}, g_3(x) = \begin{bmatrix} 0_{1 \times 10} \\ \frac{d}{I_y} \\ 0 \end{bmatrix}, g_4(x) = \begin{bmatrix} 0_{1 \times 11} \\ \frac{d}{I_z} \end{bmatrix} \quad (7)$$

where $V = [v_x, v_y, v_z]^\top$, d is the distance from the center of mass to the rotors, and g is the gravity constant. u_1 associated with $g_1(x)$ is the total applied thrust and $[u_2, u_3, u_4]$ associated with $[g_2(x), g_3(x), g_4(x)]$ refer to UAV rotational torque inputs. The output is expressed as follows:

$$y_1 = x, \quad y_2 = y, \quad y_3 = z, \quad y_4 = \psi. \quad (8)$$

IV. LINEAR EQUIVALENCE MODEL

In this section, the linear equivalence model of the VTOL-UAV model in (7) will be discussed. In view of (1) and (2), the VTOL-UAV nonlinear underactuated dynamics can be converted into a linear system of a chain of integrators if the input-to-state full feedback Linearization is solvable.

A. Feedback Linearization

Recalling (1), the vector relative degree can be defined as $r = [r_1, r_2, r_3, r_4]^\top$. For $\rho = 1$, one shows that $\mathcal{L}_{g_j} h_i(x) = 0$, $\forall 1 \leq j \leq 4$ and $1 \leq i \leq 4$, and hence one concludes that $r_1 = r_2 = r_3 = r_4 \neq 1$. For $\rho = 2$ and after some tedious

calculations to compute $A(x)$ one obtains:

$$A(x) = \begin{bmatrix} \mathcal{L}_{g_1} \mathcal{L}_f h_1(x) & \mathcal{L}_{g_2} \mathcal{L}_f h_1(x) & \cdots & \mathcal{L}_{g_4} \mathcal{L}_f h_1(x) \\ \mathcal{L}_{g_1} \mathcal{L}_f h_2(x) & \mathcal{L}_{g_2} \mathcal{L}_f h_2(x) & \cdots & \mathcal{L}_{g_4} \mathcal{L}_f h_2(x) \\ \vdots & \vdots & \ddots & \vdots \\ \mathcal{L}_{g_1} \mathcal{L}_f h_4(x) & \mathcal{L}_{g_2} \mathcal{L}_f h_4(x) & \cdots & \mathcal{L}_{g_4} \mathcal{L}_f h_4(x) \end{bmatrix}$$

$$= \begin{bmatrix} \frac{-(c_\phi c_\theta s_\psi + s_\phi s_\psi)}{m} & 0 & 0 & 0 \\ \frac{-(c_\phi c_\theta s_\psi + s_\phi s_\psi)}{m} & 0 & 0 & 0 \\ \frac{-c_\theta c_\phi}{m} & 0 & 0 & 0 \\ 0 & 0 & \frac{d}{I_y} s_\phi \sec \theta & \frac{1}{I_z} c_\phi \sec \theta \end{bmatrix} \quad (9)$$

It becomes apparent that $A(x)$ is singular and in view of (2) the full input-to-state feedback linearization using the control input is unsolvable. As such, some modifications are necessary to render the nonlinear model dynamics in (7) accounting for the full input-to-state feedback linearizable form which is the focus of the next subsection.

B. Dynamic Feedback Linearization (DFL)

DFL also known as the dynamic extension algorithm, is comprehensively discussed in ([20], Chapter 5). By analyzing the decoupling matrix $A(x)$ in (9), it is obvious that the applied torque inputs u_2 , u_3 , and u_4 are the main challenge since they do not appear in any of the first three outputs (x, y, z) resulting in $A(x)$ singularity. One way to address this issue is by adding a differential delay to the total thrust, u_1 . This way, the integrator would allow u_2 , u_3 , and u_4 to appear in the zero-column of $A(x)$ in (9). By setting u_1 to be the output of two integrators adding two new states such that $u_1 = \zeta$, $\dot{\zeta} = \zeta$ and $\ddot{\zeta} = \mathcal{U}_1$, resulting in a new vector fields $\bar{f}(\bar{x})$, $\bar{g}_1(\bar{x})$, $\bar{g}_2(\bar{x})$, $\bar{g}_3(\bar{x})$ and $\bar{g}_4(\bar{x})$ as well as new control signals \mathcal{U}_1 while the three control torques will remain unchanged $\mathcal{U}_2 = u_2$, $\mathcal{U}_3 = u_3$, and $\mathcal{U}_4 = u_4$. The extended dynamics of the VTOL-UAV will have a new state vector $\bar{x} = [p_x, p_y, p_z, \phi, \theta, \psi, v_x, v_y, v_z, \zeta, \dot{\zeta}, \dot{\phi}, \dot{\theta}, \dot{\psi}]^\top \in \mathbb{R}^{14}$ and the new system have $\bar{n} = 14$. Based on (2), $\sum_{r=1}^4 \bar{r} = 14 = \bar{n}$ implies that the full input-to-state feedback linearization is solvable for the extended UAV dynamic model using the feedback controller:

$$u = \underbrace{\begin{bmatrix} \bar{a}_{11} & \bar{a}_{12} & \bar{a}_{13} & \bar{a}_{14} \\ \bar{a}_{21} & \bar{a}_{22} & \bar{a}_{23} & \bar{a}_{24} \\ \bar{a}_{31} & \bar{a}_{32} & \bar{a}_{33} & \bar{a}_{34} \\ \bar{a}_{41} & \bar{a}_{42} & \bar{a}_{43} & \bar{a}_{44} \end{bmatrix}}_{\bar{A}^{-1}(x)} \left(\begin{bmatrix} -\mathcal{L}_{\bar{f}}^4 h_1(\bar{x}) \\ -\mathcal{L}_{\bar{f}}^4 h_2(\bar{x}) \\ -\mathcal{L}_{\bar{f}}^4 h_3(\bar{x}) \\ -\mathcal{L}_{\bar{f}}^2 h_4(\bar{x}) \end{bmatrix} + \begin{bmatrix} v_1 \\ v_2 \\ v_3 \\ v_4 \end{bmatrix} \right) \quad (10)$$

where:

$$\bar{a}_{11} = m(s_{\bar{x}_4} s_{\bar{x}_6} + c_{\bar{x}_4} c_{\bar{x}_6} s_{\bar{x}_5}) \quad \bar{a}_{31} = \frac{I_y m c_{\bar{x}_5} c_{\bar{x}_6}}{d\bar{x}_{13}}$$

$$\bar{a}_{12} = m(c_{\bar{x}_4} s_{\bar{x}_5} s_{\bar{x}_6} - m c_{\bar{x}_6} s_{\bar{x}_4}) \quad \bar{a}_{32} = \frac{I_y m c_{\bar{x}_5} s_{\bar{x}_6}}{d\bar{x}_{13}}$$

$$\bar{a}_{21} = \frac{I_x m (c_{\bar{x}_4} s_{\bar{x}_6} - c_{\bar{x}_6} s_{\bar{x}_4} s_{\bar{x}_5})}{d\bar{x}_{13}} \quad \bar{a}_{33} = \frac{-I_y m s_{\bar{x}_5}}{d\bar{x}_{13}}$$

$$\bar{a}_{22} = \frac{I_x m (c_{\bar{x}_4} c_{\bar{x}_6} - s_{\bar{x}_4} s_{\bar{x}_5} s_{\bar{x}_6})}{d\bar{x}_{13}} \quad \bar{a}_{41} = \frac{-I_z m c_{\bar{x}_5} c_{\bar{x}_6} t_{\bar{x}_4}}{d\bar{x}_{13}}$$

$$\bar{a}_{23} = \frac{I_x m c_{\bar{x}_5} s_{\bar{x}_4}}{d\bar{x}_{13}} \quad \bar{a}_{42} = \frac{-I_z m c_{\bar{x}_5} s_{\bar{x}_4} s_{\bar{x}_6}}{d\bar{x}_{13} c_{\bar{x}_4}}$$

$$\bar{a}_{43} = \frac{-I_z m s_{\bar{x}_5} t_{\bar{x}_4}}{d\bar{x}_{13}} \quad \bar{a}_{44} = \frac{-I_z m c_{\bar{x}_5}}{d\bar{x}_4}$$

$$\bar{a}_{13} = m x_{\bar{x}_4} c_{\bar{x}_5} \quad \bar{a}_{14} = \bar{a}_{24} = \bar{a}_{34} = 0$$

Thus, one can verify that the invertibility of the decoupling matrix is guaranteed by constraining the pitch angle θ such that $-\frac{\pi}{2} < \theta < \frac{\pi}{2}$ and the roll angle such that $-\frac{\pi}{2} < \phi < \frac{\pi}{2}$. The exact expressions of $\mathcal{L}_f^4 h_1(\bar{x})$, $\mathcal{L}_f^4 h_2(\bar{x})$, $\mathcal{L}_f^4 h_3(\bar{x})$ and $\mathcal{L}_f^2 h_4(\bar{x})$ will not be stated due to page limitations.

V. PROPOSED SCHEME

The key feature of obstacle avoidance control scheme is the safety constraints represented by the CBF. In [3], the authors proposed CBF \mathcal{H}_k representing a safety metric as the distance between the moving object and the obstacle. The sufficient and necessary conditions for the safe maneuvers are based on the usage of class \mathcal{K}_∞ function similar to Lyapunov functions such that $\dot{\mathcal{H}}(x, u) \geq -\kappa(\mathcal{H}(x)) \iff C$ is invariant. The proposed scheme makes use of the CBF concepts in the MPC formulation cascaded by dynamic feedback controller defined in (10). The motivation for using the cascaded scheme will be unlocking the usage of a linear MPC with all its merit compared to the nonlinear MPC in terms of computational cost and ease of stability guarantees.

Lemma 3. (States mapping of VTOL-UAV in MPC-DFL scheme) Recall the VTOL-UAV model dynamics in (7). Using the control input in (10), the optimization problem of the MPC in the cascaded scheme of MPC-DFL can be formulated on a linear equivalent model dynamics as $\dot{z} = A_z z + B_z v$ with the following state and input mapping:

$$\begin{aligned} z_1 &= x, & z_8 &= \ddot{y} \\ z_2 &= \dot{x}, & z_9 &= z \\ z_3 &= \ddot{x}, & z_{10} &= \dot{z} \\ z_4 &= \ddot{x}, & z_{11} &= \ddot{z} \\ z_5 &= y, & z_{12} &= \ddot{z} \\ z_6 &= \dot{y}, & z_{13} &= \psi \\ z_7 &= \ddot{y}, & z_{14} &= \dot{\psi} \end{aligned} \quad (11)$$

$$\begin{bmatrix} v_1 \\ v_2 \\ v_3 \\ v_4 \end{bmatrix} = \bar{A}(\bar{x}) \begin{bmatrix} u_1 \\ u_2 \\ u_3 \\ u_4 \end{bmatrix} + \begin{bmatrix} \mathcal{L}_f^4 h_1(\bar{x}) \\ \mathcal{L}_f^4 h_2(\bar{x}) \\ \mathcal{L}_f^4 h_3(\bar{x}) \\ \mathcal{L}_f^2 h_4(\bar{x}) \end{bmatrix} \quad (12)$$

Proof. The detailed proof is omitted due to the limited page numbers. However, using the state mapping from z to x in (11), having the derivatives of z states, and applying the controller in (10), one finds the following linear system:

$$\dot{z} = A_z z + B_z v. \quad (13)$$

$$y_z = C_z z. \quad (14)$$

where

$$A_z = \begin{bmatrix} A_{z1} & 0_{4 \times 4} & 0_{4 \times 4} & 0_{4 \times 2} \\ 0_{4 \times 4} & A_{z1} & 0_{4 \times 4} & 0_{4 \times 2} \\ 0_{4 \times 4} & 0_{4 \times 4} & A_{z1} & 0_{4 \times 2} \\ 0_{2 \times 4} & 0_{2 \times 4} & 0_{2 \times 4} & A_{z2} \end{bmatrix}, B_z = \begin{bmatrix} B_{1z} \\ B_{2z} \\ B_{3z} \\ B_{4z} \end{bmatrix}$$

$$C_z = \text{diag}(C_{z1}, C_{z1}, C_{z1}, C_{z2})$$

with

$$\begin{aligned} A_{1z} &= \begin{bmatrix} 0_{3 \times 1} & \mathbf{I}_3 \\ 0 & 0_{1 \times 3} \end{bmatrix}, A_{2z} = \begin{bmatrix} 0 & 1 \\ 0 & 0 \end{bmatrix}, \\ B_{1z} &= \begin{bmatrix} 0_{3 \times 1} & 0_{3 \times 3} \\ 1 & 0_{1 \times 3} \end{bmatrix}, B_{2z} = \begin{bmatrix} 0_{3 \times 1} & 0_{3 \times 1} & 0_{3 \times 2} \\ 0 & 1 & 0_{1 \times 2} \end{bmatrix} \\ B_{3z} &= \begin{bmatrix} 0_{3 \times 2} & 0_{3 \times 1} & 0_{3 \times 1} \\ 0_{1 \times 2} & 1 & 0 \end{bmatrix}, B_{4z} = \begin{bmatrix} 0_{1 \times 3} & 0 \\ 0_{1 \times 3} & 1 \end{bmatrix}, \\ C_{1z} &= [1 \ 0 \ 0 \ 0], C_{2z} = [1 \ 0] \end{aligned}$$

To implement MPC, the linear equivalent model in (13) and (14), is discretized as follows:

$$z_d(k+1|k) = A_d z_d(k) + B_d v_d(k). \quad (15)$$

where δ is the sampling period, $A_d = (I + \delta A_z)$, $B_d = \delta B_z$. The associated QCQP problem can be formulated as:

$$J = \min_{v_d(k)} \sum_{i=0}^{N-1} [z_d(k+i|k)^\top Q z_d(k+i|k) + v_d(k+i|k)^\top R v_d(k+i|k)] + z_d(N|k)^\top \bar{Q} z_d(N|k) \quad (16)$$

subject to

$$z_d(k+1) = A_d z_d(k) + B_d v_d(k), \forall k = 0, \dots, N-1. \quad (17)$$

$$\begin{bmatrix} \underline{z}_1 \\ \underline{z}_5 \\ \underline{z}_9 \\ \underline{z}_{13} \end{bmatrix} \leq \begin{bmatrix} z_1 \\ z_5 \\ z_9 \\ z_{13} \end{bmatrix} \leq \begin{bmatrix} \bar{z}_1 \\ \bar{z}_5 \\ \bar{z}_9 \\ \bar{z}_{13} \end{bmatrix}, \forall k = 0, \dots, N-1. \quad (18)$$

$$v_{\min} \leq v_d \leq v_{\max}, \forall k = 0, \dots, N-1. \quad (19)$$

$$\Delta \mathcal{H}(z_d(k+1)) \geq -\gamma \mathcal{H}(z_d(k)), k = 0, \dots, N-1. \quad (20)$$

$$v_{\min} \leq K(A_d + B_d K)^i z_d(k+N|k) \leq v_{\max}, \quad \forall k = 0, \dots, N_c. \quad (21)$$

$$\begin{bmatrix} \underline{z}_1 \\ \underline{z}_5 \\ \underline{z}_9 \\ \underline{z}_{13} \end{bmatrix} \leq (A_d + B_d K)^i z_d(k+N|k) \leq \begin{bmatrix} \bar{z}_1 \\ \bar{z}_5 \\ \bar{z}_9 \\ \bar{z}_{13} \end{bmatrix}, \quad \forall k = 0, \dots, N_c. \quad (22)$$

where N is the prediction horizon, N_c is the constraint checking horizon, Q and R are the states and inputs weight matrices, respectively, and \bar{Q} is the terminal weight matrix. The expression in (17) is the dynamical constraint of the linear equivalent model. Note that \underline{z}_\times and \bar{z}_\times refer to the minimum and maximum value associated with the subscript \times , respectively. The expression in (19) represents control input constraints of z dynamics. In the view of the input constraint mapping in (10), it is clear that there is a nonlinear relation between the control inputs of \bar{x} and z dynamics. However, one can easily use $\bar{A}^{-1}(\bar{x})$, $\mathcal{L}_f^4 h_1(\bar{x})$, $\mathcal{L}_f^4 h_2(\bar{x})$, $\mathcal{L}_f^4 h_3(\bar{x})$, and $\mathcal{L}_f^2 h_4(\bar{x})$ to verify the boundedness of v will guarantee boundedness of u . Let us propose the following control barrier

function:

$$\mathcal{H}_k = (z_1 - x_{\text{obs}})^2 + (z_5 - y_{\text{obs}})^2 + (z_9 - z_{\text{obs}})^2 - r_{\text{obs}}^2 \quad (23)$$

where x_{obs} , y_{obs} , and z_{obs} describe x , y and z coordinates of the obstacle, respectively and $0 < \gamma \leq 1$. The expression in (20) defines the proposed safety constraint based on \mathcal{H}_k , where it forces the forward invariance of a safe set \mathcal{C}_k [3]. Fig. 2 shows the proposed MPC-CBF-DFL scheme, where the mapping function $\Phi(\bar{x})$ represents the state mapping of (11). $\Phi(\bar{x})$ converts the feedback signals of the states in \bar{x} dynamics to z where the optimization problem of MPC-CBF is solved providing the values of v to be given to the DFL controller.

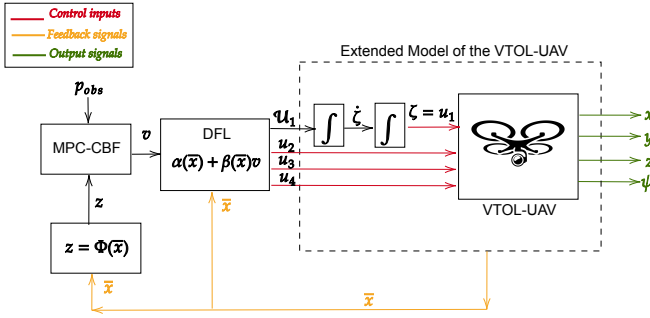


Fig. 2: MPC-CBF-DFL scheme for the VTOL-UAV.

From (20), the level set of CBF constraints is defined by

Assumption 1. *The optimization problem (16)-(22) is feasible for the initial time $k = 0$.*

Assumption 2. *The VTOL-UAV pitch angle θ and roll angle ϕ are constraint by $-\frac{\pi}{2} < \theta < \frac{\pi}{2}$ and $-\frac{\pi}{2} < \phi < \frac{\pi}{2}$ such that the inverse of the decoupling matrix in (10) is nonsingular.*

Theorem 1. *(Asymptotic convergence of MPC-CBF-DFL of VTOL-UAV model) The Dynamics of the VTOL-UAV model in (7) are asymptotically stable and the obstacles are avoided using MPC-CBF-DFL scheme if Assumptions 1 and 2 hold true and the terminal weight in (24) is selected to be equivalent to the infinite horizon cost where*

$$\sum_{i=0}^{\infty} (\|z(i)\|_Q^2 + \|v(i)\|_R^2) = z^T(0)\bar{Q}z(0) \quad (24)$$

and

$$\bar{Q} - (A_d + B_dK)^T \bar{Q} (A_d + B_dK) = Q + K^T R K. \quad (25)$$

such that the optimization problem in (16)-(22) is recursively feasible given the K is stabilizing $(A_d + B_dK)^i \forall i = 1, \dots, N_c$ and $\mathcal{H}((A_d + B_dK)z_d) > (1 - \gamma)\mathcal{H}(z_d) \forall z_d \in \mathcal{Z}_f$ with sufficiently large N_c and $0 < \gamma \leq 1$.

Proof. Recall the linear equivalent model of the VTOL-UAV in (13) and (14), and the cost function in (16). The use of the terminal cost function \bar{Q} to solve the Lyapunov function in (25) will render the optimal cost function for the next time step $k + 1$ and thereby $J^*(k + 1)$ is equal to $J^*(k) - (\|z_d(k)\|_Q^2 + \|v(k)\|_R^2)$. Hence, it can be concluded that $J^*(k + 1) \rightarrow 0$ as $k \rightarrow 0$. From (11), one

finds as $z \rightarrow 0$ and $\bar{x} \rightarrow 0$ results in asymptotic convergence. We prove the recursive stability using the classical terminal constraints [23]. Let $\tilde{v}_d(k + 1)$ denote the input sequence at time $k + 1$ corresponding to the optimal prediction at time k . For feasible $\tilde{v}_d(k + 1)$ the N th element (the tail of $v_d^*(k + N|k) = Kz_d^*(k + N|k)$ is required to satisfy the terminal constraint. This is equivalent to the constraints on the terminal state prediction $z_d(k + N|k) \in \mathcal{Z}_f$, where \mathcal{Z}_f is the terminal set. The necessary and sufficient conditions for the predictions generated by the tail $\tilde{v}_d(k + 1)$ are feasible at time $k + 1$ is to control \mathcal{Z}_f and achieve safe invariance. The terminal set \mathcal{Z}_f is control invariant if $(A_d + B_dK)z_d(k + N|k) \in \mathcal{Z}_f \forall z_d(k + N|k) \in \mathcal{Z}_f$. The terminal set \mathcal{Z}_f is safe invariant if $\Delta\mathcal{H}(z_d(k + 1|N)) \geq -\gamma\mathcal{H}(z_d(k|N)) \forall z_d(k + N|k) \in \mathcal{Z}_f$. To render \mathcal{Z}_f control invariant, we need to verify that

$$v_{\max} \leq K(A_d + B_dK)^i z_d(k + N|k) \leq v_{\max} \quad (26)$$

$$\begin{bmatrix} z_1 \\ z_5 \\ z_9 \\ z_{13} \end{bmatrix} \leq (A_d + B_dK)^i z_d(k + N|k) \leq \begin{bmatrix} \bar{z}_1 \\ \bar{z}_5 \\ \bar{z}_9 \\ \bar{z}_{13} \end{bmatrix} \quad \forall i \geq 0 \quad (27)$$

one can design K to render $(A_d + B_dK)^i$ stable such that the norm of $|\lambda(A_d + B_dK)| < 1$. To render \mathcal{Z}_f safe invariant, the constraint (20) will impose that $\mathcal{H}(z_d(k + 1|N)) - \mathcal{H}(z_d(k|N)) \geq -\gamma\mathcal{H}(z_d(k|N))$ and as a result with $0 < \gamma \leq 1$. We have $\mathcal{H}(z_d(k + 1|N)) > \mathcal{H}(z_d(k|N))$. From (20), if $z_d(N|0) \in \mathcal{Z}_f$ such that $\mathcal{H}(z_d(N|0)) \geq 0$. One can design K such that $\mathcal{H}((A_d + B_dK)z_d) > (1 - \gamma)\mathcal{H}(z_d)$ with $0 < \gamma \leq 1$ proving the safety invariance of \mathcal{Z}_f . ■

Assumption 1 provides the initial feasibility conditions at $k = 0$ where Theorem 1 guarantees the feasibility for the next time steps. We can define the terminal constraint set as $\mathcal{Z}_f(N_c) = \{z_d : v_{\min} \leq K(A_d + B_dK)^i z_d \leq v_{\max}, i = 0, 1, \dots, N_c\}$. By choosing sufficiently large N_c , the allowable operating region of the MPC law will be increased satisfying all the constraints. Note that the constraints in (21) and (22) are extra computational burden specially with large N_c which is needed to maintain the feasibility (visit Theorem 1). However, the constraints in (21) and (22) are linear constraints, where the QCQP presented in (16)-(22) can be solved efficiently by off-the-shelf solvers. In the next section, the proposed scheme will be tested with respect to the baseline of having constraint of the Euclidean distance (denoted as MPC-EC-DFL). Since the chosen CBF function in (23) is equal to Euclidean distance, the new safety constraint in (20) will be $\mathcal{H}(x_k) > 0$.

VI. NUMERICAL RESULTS

The QCQP problem in (16)-(22) was solved using Interior Point OPTimizer (IPOPT) in MATLAB. The proposed scheme was tested with a sampling time of $\delta = 0.05$ sec where the continuous dynamics in (7) and the control input in (10) were numerically integrated using 4th Order Runge Kutta Method and $\delta = 0.05$ sec. The VTOL-UAV parameters are defined as follows: $m = 0.7$ kg, $d = 0.3$ m, $I_x = I_y = I_z = 1.241$ kg/m². The VTOL-UAV started from the initial position ($x = 7$, $y = 7$, and $z = 0$) meters and $\psi = 0$ rad. The UAV moved

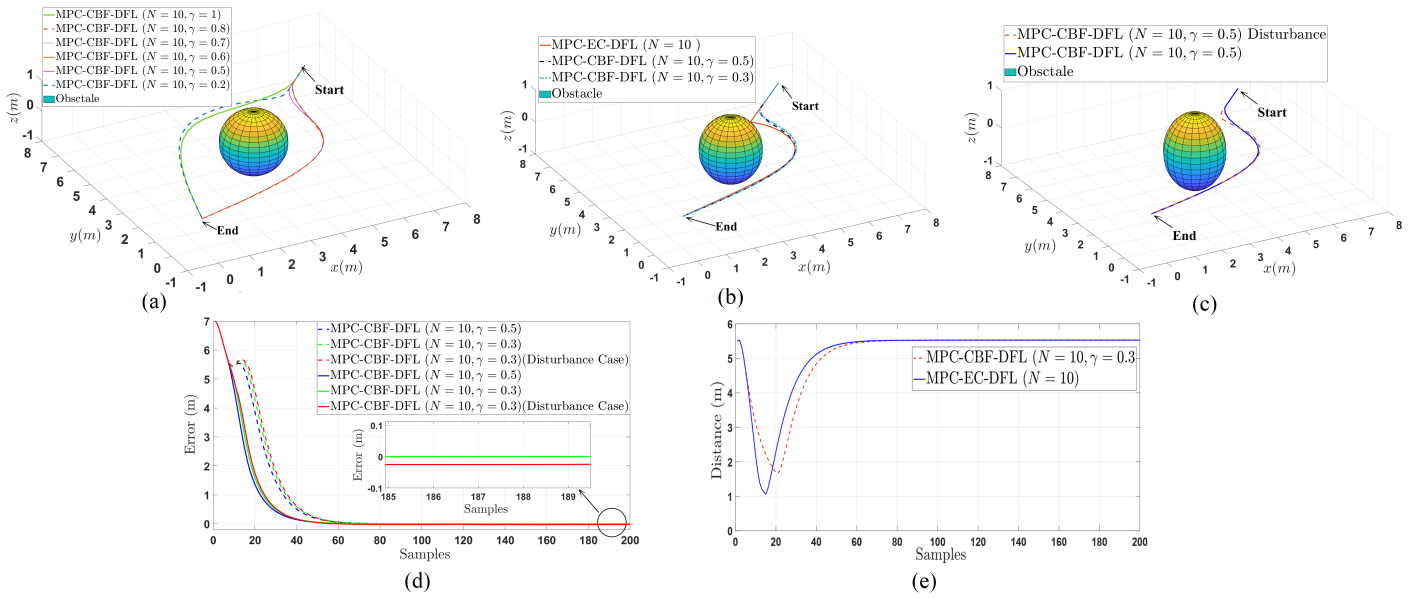


Fig. 3: Output performance of MPC-CBF-DFL scheme: (a) illustrates the safe navigation of the VTOL-UAV against a spherical Obstacle with different pairs of N and γ ; (b) presents a comparison between MPC-CBF-DF vs. MPC-ED-DF schemes; (c) shows the trajectories of the proposed scheme against a noisy feedback signal corrupted by a Gaussian noise; (d) shows the error signals where dashed-line and solid-line refer to the x and y errors, respectively; (e) depicts the distance between the VTOL-UAV and the obstacle (MPC-CBF-DF vs. MPC-ED-DF schemes)

toward the origin against a sphere obstacle placed at the middle of the map.

Fig. 3.(a) shows the effect of γ in the evolution of the VTOL-UAV trajectory. By setting a small value of γ , $\mathcal{H}(x_{k+1})$ will be significantly greater than $\mathcal{H}(x_k)$, which simply means a bigger safety metric for the next time step $k+1$. Nonetheless, Fig. 3.(a) illustrates the merit of using CBF for obstacle avoidance, where stronger safety measures with a lower value of γ would lead to lower prediction horizons demonstrating the effectiveness of employing CBF. The performance of the proposed scheme MPC-CBF-DFL against the baseline of Euclidean distance constraint (MPC-ED-DFL) is presented in Fig. 3.(b). MPC-ED-DFL scheme (demonstrated in blue line) in Fig. 3.(b) deviates from the obstacle once it gets closer to it. In contrast, using the same prediction horizon the proposed MPC-CBF-DFL (plotted in blue and green lines) deviates from the obstacle ahead, since the proposed scheme relies on the availability of the feedback signals. Fig. 3.(c) illustrates the robustness of the proposed scheme against noisy feedback signals corrupted by a Gaussian noise with zero mean and variance of 0.05. Fig. 3.(d) shows the asymptotic convergence of the error of x and y to the origin, while in the case of disturbance the error convergence to the neighborhood of the origin. Fig. 3.(e) depicts the distance between the VTOL-UAV and the obstacle using the proposed MPC-CBF-DFL scheme and compared to the MPC-ED-DFL scheme.

VII. CONCLUSION

In this paper, a cascaded scheme of Dynamic Feedback Linearization (DFL) and Model prediction Control (MPC)

was proposed to achieve safe navigation of Vertical Take-off and Landing (VTOL) Unmanned Aerial Vehicles (UAVs). The MPC was formulated on the linear equivalent model rendered by the DFL. The proposed scheme showed a strong theoretical guarantee for closed-loop stability and recursive feasibility based on Linear MPC stability analysis. Numerical simulations illustrated successful obstacle-free navigation paths where fast and easy implementation can be achieved with a theoretical guarantee of convergence. The utilization of the Control Barrier Functions (CBF) within the safety constraints improved the obstacle avoidance maneuvers with respect to the constraints based on Euclidean distances. Numerical results illustrated robustness of the proposed MPC-ED-DFL scheme.

REFERENCES

- [1] H. A. Hashim, "Exponentially stable observer-based controller for vtol-uavs without velocity measurements," *International Journal of Control*, vol. 96, no. 8, pp. 1946–1960, 2023.
- [2] H. A. Hashim, A. E. Eltoukhy, and A. Odry, "Observer-based controller for vtol-uavs tracking using direct vision-aided inertial navigation measurements," *ISA transactions*, vol. 137, pp. 133–143, 2023.
- [3] A. D. Ames, S. Coogan, M. Egerstedt, G. Notomista, K. Sreenath, and P. Tabuada, "Control barrier functions: Theory and applications," in *2019 18th European control conference (ECC)*. IEEE, 2019, pp. 3420–3431.
- [4] M. Nagumo, "Über die lage der integralkurven gewöhnlicher differentialgleichungen," *Proceedings of the Physico-Mathematical Society of Japan. 3rd Series*, vol. 24, pp. 551–559, 1942.
- [5] F. Blanchini, "Set invariance in control," *Automatica*, vol. 35, no. 11, pp. 1747–1767, 1999.
- [6] A. D. Ames, X. Xu, J. W. Grizzle, and P. Tabuada, "Control barrier function based quadratic programs for safety critical systems," *IEEE Transactions on Automatic Control*, vol. 62, no. 8, pp. 3861–3876, 2016.
- [7] A. Singletary and et al, "Comparative analysis of control barrier functions and artificial potential fields for obstacle avoidance," in *2021 IEEE/RSJ International Conference on Intelligent Robots and Systems (IROS)*. IEEE, 2021, pp. 8129–8136.

- [8] D. Zhang, G. Yang, and R. P. Khurshid, "Haptic teleoperation of uavs through control barrier functions," *IEEE transactions on haptics*, vol. 13, no. 1, pp. 109–115, 2020.
- [9] Y. Yoon, J. Shin, H. J. Kim, Y. Park, and S. Sastry, "Model-predictive active steering and obstacle avoidance for autonomous ground vehicles," *Control Engineering Practice*, vol. 17, no. 7, pp. 741–750, 2009.
- [10] J. V. Frasch, A. Gray, M. Zanon, H. J. Ferreau, S. Sager, F. Borrelli, and M. Diehl, "An auto-generated nonlinear mpc algorithm for real-time obstacle avoidance of ground vehicles," in *2013 European Control Conference (ECC)*. IEEE, 2013, pp. 4136–4141.
- [11] J. Zeng, B. Zhang, and K. Sreenath, "Safety-critical model predictive control with discrete-time control barrier function," in *2021 American Control Conference (ACC)*. IEEE, 2021, pp. 3882–3889.
- [12] V. Turri, A. Carvalho, H. E. Tseng, K. H. Johansson, and F. Borrelli, "Linear model predictive control for lane keeping and obstacle avoidance on low curvature roads," in *16th international IEEE conference on intelligent transportation systems*. IEEE, 2013, pp. 378–383.
- [13] T. D. Son and Q. Nguyen, "Safety-critical control for non-affine nonlinear systems with application on autonomous vehicle," in *2019 IEEE 58th Conference on Decision and Control (CDC)*. IEEE, 2019, pp. 7623–7628.
- [14] U. Rosolia and A. D. Ames, "Multi-rate control design leveraging control barrier functions and model predictive control policies," *IEEE Control Systems Letters*, vol. 5, no. 3, pp. 1007–1012, 2020.
- [15] R. Grandia, A. J. Taylor, A. D. Ames, and M. Hutter, "Multi-layered safety for legged robots via control barrier functions and model predictive control," in *2021 IEEE International Conference on Robotics and Automation (ICRA)*. IEEE, 2021, pp. 8352–8358.
- [16] S. Liu, J. Zeng, K. Sreenath, and C. A. Belta, "Iterative convex optimization for model predictive control with discrete-time high-order control barrier functions," in *2023 American Control Conference (ACC)*. IEEE, 2023, pp. 3368–3375.
- [17] H. L. N. N. Thanh and S. K. Hong, "Completion of collision avoidance control algorithm for multicopters based on geometrical constraints," *IEEE Access*, vol. 6, pp. 27 111–27 126, 2018.
- [18] H. Chen, K. Chang, and C. S. Agate, "Uav path planning with tangent-plus-lyapunov vector field guidance and obstacle avoidance," *IEEE Transactions on Aerospace and Electronic Systems*, vol. 49, no. 2, pp. 840–856, 2013.
- [19] M. Odelga, P. Stegagno, and H. H. Bühlhoff, "Obstacle detection, tracking and avoidance for a teleoperated uav," in *2016 IEEE international conference on robotics and automation (ICRA)*. IEEE, 2016, pp. 2984–2990.
- [20] A. Isidori, *Nonlinear control systems: an introduction*. Springer, 1985.
- [21] H. A. Hashim, "Special orthogonal group $so(3)$, euler angles, angle-axis, rodriguez vector and unit-quaterrion: Overview, mapping and challenges," *arXiv preprint arXiv:1909.06669*, 2019.
- [22] S. Bouabdallah, "Design and control of quadrotors with application to autonomous flying," Eplf, Tech. Rep., 2007.
- [23] P. O. Scokaert and J. B. Rawlings, "Infinite horizon linear quadratic control with constraints," *IFAC Proceedings Volumes*, vol. 29, no. 1, pp. 5905–5910, 1996.